The NMR Structure of Human β-Defensin-2 Reveals a Novel α-Helical Segment[†,‡]

Monali V. Sawai,[§] Hong Peng Jia,[∥] Lide Liu,[⊥] Vladimir Aseyev,[@] John M. Wiencek,[@] Paul B. McCray, Jr.,[∥] Tomas Ganz,[⊥] William R. Kearney,[#] and Brian F. Tack*[,§]

Departments of Microbiology and Pediatrics and NMR Facility, The University of Iowa College of Medicine, Iowa City, Iowa 52242, Department of Chemical and Biochemical Engineering, The University of Iowa, Iowa City, Iowa 52242, and Department of Medicine, University of California School of Medicine, Los Angeles, California 90095

Received November 1, 2000; Revised Manuscript Received February 13, 2001

ABSTRACT: Human β-defensin-2 (HBD-2) is a member of the defensin family of antimicrobial peptides. HBD-2 was first isolated from inflamed skin where it is posited to participate in the killing of invasive bacteria and in the recruitment of cells of the adaptive immune response. Static light scattering and two-dimensional proton nuclear magnetic resonance spectroscopy have been used to assess the physical state and structure of HBD-2 in solution. At concentrations of ≤2.4 mM, HBD-2 is monomeric. The structure is amphiphilic with a nonuniform surface distribution of positive charge and contains several key structural elements, including a triple-stranded, antiparallel β-sheet with strands 2 and 3 in a β-hairpin conformation. A β-bulge in the second strand occurs at Gly28, a position conserved in the entire defensin family. In solution, HBD-2 exhibits an α-helical segment near the N-terminus that has not been previously ascribed to solution structures of α-defensins or to the β-defensin BNBD-12. This novel structural element may be a factor contributing to the specific microbicidal or chemokine-like properties of HBD-2.

Defensins are small cationic antimicrobial peptides that contribute to host defense in multicellular organisms (*1*). Three intramolecular disulfide bonds are conserved throughout the defensin family and provide stability to defensin tertiary structures. Mammalian α- and β-defensins differ in the pairing of six invariant cysteine residues (*2*, *3*). The disulfide connectivity in α-defensins is 1−6, 2−4, and 3−5, whereas that in β-defensins is 1−5, 2−4, and 3−6. The high net positive charge of defensins facilitates their electrostatic interaction with polyanionic surfaces of bacterial cells. Defensins exert their antimicrobial activity by permeabilization of bacterial membranes followed by interactions with additional, but as yet uncharacterized, intracellular targets (*1*, *4*). Human β-defensin-2 (HBD-2),[1] a 41-residue peptide, was first isolated from inflamed skin of patients with psoriasis where it was found at micromolar levels (*5*, *6*). Subsequent studies have shown the peptide to be secreted at mucosal surfaces of the respiratory tract, oral cavity, and intestine (*7*−*9*). Transcription of the HBD-2 gene is enhanced by proinflammatory cytokines such as interleukin-1β, tumor necrosis factor-α, and bacterial lipopolysaccharide (*7*−*10*). At nanomolar concentrations, HBD-2 attracts immature dendritic cells and memory T-cells, a chemokine-like activity mediated through the CCR6 receptor (*11*). Thus, HBD-2 appears an important effector molecule of innate immunity and an early activating signal in the recruitment of cells that mediate an adaptive immune response.

To date, NMR solution structures are available for three mammalian α-defensins. These include the human neutrophil peptide HNP-1 (*14*, *15*) and the rabbit neutrophil defensins NP-5 (*12*, *13*) and NP-2 (*14*, *15*). The solution structure of bovine neutrophil β-defensin-12 (BNBD-12) has also been determined by NMR (*16*). The first defensin crystal structure was of human neutrophil α-defensin HNP-3 (*17*). From these studies, a triple-stranded, antiparallel β-sheet with strands 2 and 3 involved in a β-hairpin has emerged as a common structural feature in both α- and β-defensins. However, differences in the antimicrobial spectrum and activity of defensins remain largely unexplained. Recently, the X-ray structure of the first human β-defensin HBD-2 was published (*18*). While the general shape and charge distributions were similar to those of previously determined defensin structures, HBD-2 contained an additional structural element in the form of an α-helical region. In the crystalline state, HBD-2 was dimeric and exhibited higher-order oligomeric structure. Our

[†] This work was supported in part by funds from the NHLBI (Grant SCOR HL42385 to P.B.M. and B.F.T.), the CFF (Grant 97ZO to P.B.M. and B.F.T.), and the NIH (Grant HL46809 to T.G. and L.L.) and the University of Iowa College of Medicine (W.R.K.).

[‡] The NMR data and the coordinates of the final 20 structures of the first N-terminal hydrogen bonding model have been deposited in the RCSB Protein Data Bank (PDB entry 1FQQ). The coordinates of the final 20 structures of the second N-terminal hydrogen bonding model will be available on request.

* To whom correspondence should be addressed. Phone: (319) 335-8891. Fax: (319) 353-3038. E-mail: brian-tack@uiowa.edu.

[§] Department of Microbiology, The University of Iowa College of Medicine.

[∥] Department of Pediatrics, The University of Iowa College of Medicine.

[⊥] University of California School of Medicine.

[@] The University of Iowa.

[#] NMR Facility, The University of Iowa College of Medicine.

[1] Abbreviations: BNBD-12, bovine neutrophil β-defensin-12; DQF-COSY, double-quantum-filtered correlation spectroscopy; HBD-1, human β-defensin-1; HBD-2, human β-defensin-2; HNP-1, human neutrophil peptide-1; HNP-3, human neutrophil peptide-3; NMR, nuclear magnetic resonance; NOESY, nuclear Overhauser effect spectroscopy; NP-2, rabbit neutrophil peptide-2; NP-5, rabbit neutrophil peptide-5; rmsd, root-mean-square deviation; TOCSY, total correlation spectroscopy.

10.1021/bi002519d CCC: $20.00
Published on Web 03/09/2001

analysis of HBD-2 in solution at pH 3.7 or 6.4 by static light scattering and two-dimensional NMR has established that the peptide is monomeric in the concentration range of 0.5−2.4 mM and displays a novel α-helical segment. Thus, our data establish that the helical portion of HBD-2 is an inherent structural feature of the monomeric form of the peptide and not a product of higher-order oligomeric structures that are evident from crystallographic studies.

MATERIALS AND METHODS

Peptide. HBD-2 utilized in these studies was obtained using an insect cell/baculovirus protein expression system as previously described for HBD-1 and other defensins (*19*). The homogeneity of the preparation was indicated by monodisperse behavior on capillary zone electrophoresis at pH 3.0 and by high-pressure liquid chromatography utilizing a 1000 μm inside diameter column (MIC-25-05-C18P3) provided by LC Packings (San Francisco, CA). Further confirmation of the structure was provided by both chemical and immunological methods. Mass measurements were performed on a Hewlett-Packard model 1100 MSD instrument equipped with an electrospray ionization source. The calculated mass for the fully oxidized form of HBD-2 is 4328.2 Da. The observed mass for the material used in these studies was 4328.2 ± 0.4 Da. Compositional analysis and measurement of the mass per unit volume for purposes of determining an extinction coefficient were performed with a Beckman 6300 amino acid analyzer. An extinction coefficient of 0.43 mL mg^{-1} cm^{-1} was calculated from the absorbance at 280 nm of HBD-2 solutions of known concentrations. Western analysis was performed as previously described on urea−acetic acid gels (*19*) or by SDS gel electrophoresis in precast Novex 16% Tricine gels using a previously described rabbit anti-human HBD-2 antiserum (*19*).

Light Scattering Experiments. For light scattering studies, HBD-2 solutions of different concentrations were prepared in 0.05 M NaH_2PO_4 buffer (pH 3.7) and 0.05 M Na_2HPO_4 buffer (pH 6.4). Static and dynamic light scattering measurements were conducted using an ALV/SP-125 compact goniometer and an ALV-5000/E digital correlator. A diode-pumped, solid-state laser (COHERENT, DPSS532-400) operating at 532 nm was used as a light source. Molecular masses were determined using the Debye analysis (*20*). The change in the refractive index of HBD-2 solutions was studied as a function of concentration (increment of refractive index, d*n*/d*c*) using an ALV/DR-1 differential refractometer and the laser mentioned above as the light source. The measured d*n*/d*c* value of 0.23 ± 0.01 mL/g was used for molecular mass analysis. In the dynamic light scattering experiments, the pseudo cross-correlation function of the scattered light intensity was measured in the self-beating mode (*21*). Time-correlation functions were analyzed using the regularized Laplace inversion program CONTIN (*22*). All light scattering studies were carried out at 25 °C and at a 90° scattering angle.

NMR Sample Preparation. HBD-2 (1.5 mg) was dissolved in 400 μL of 0.045 M NaH_2PO_4 buffer prepared in a 90% H_2O/10% ^2H_2O mixture (pH 3.7). This resulted in a peptide concentration of 0.9 mM.

NMR Experiments. All NMR spectra were recorded on a Varian Unity INOVA instrument operating at 500 MHz and 25 °C. DQF-COSY, TOCSY, and NOESY spectra were obtained using standard procedures. For all experiments, a 6 kHz spectral width was used in each dimension. The water signal was reduced by presaturation during a 2.5 s relaxation delay for the NOESY and TOCSY spectra and a 2 s relaxation delay for the DQF-COSY spectrum. NOESY spectra were taken at mixing times of 50, 100, 150, 300, and 400 ms. The TOCSY spectrum was collected with a mixing time of 120 ms. In the NOESY and the TOCSY spectra, the data sets were 1024 complex points in f_2 by 512 complex points in f_1, and 16 transients were averaged per f_1 increment. The DQF-COSY spectrum had a resolution of 2048 complex points in f_2 and 512 complex points in f_1 with 32 transients averaged per f_1 increment. The spectra were referenced to the water signal at 4.757 ppm. Baseline correction in f_2 was applied to NOESY spectra prior to peak volume measurement. Spectral processing and NOESY peak volume measurement were carried out using the VNMR 6.1B software package. The peak volumes measured with a mixing time of 150 ms were used in structure calculation. NOE buildup curves were found to be linear with a mixing time of 150 ms. Degenerate NOEs were excluded from structure calculation.

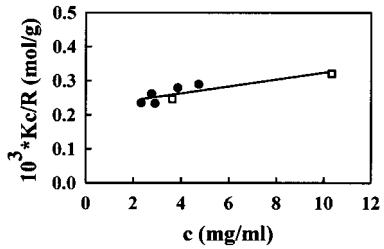

FIGURE 1: Debye plot for the static light scattering analysis of HBD-2. *K* is an optical constant; *c* is the concentration of the solution, and *R* is the Rayleigh ratio. Black circles and white squares represent the data at pH 3.7 and 6.4, respectively.

Sequential Resonance Assignment. The procedure developed by Wüthrich (*23*) was employed for sequential resonance assignment of HBD-2. Proton spin systems of individual amino acid residues were identified from the DQF-COSY and TOCSY spectra. The residues were then linked to each other in a sequential manner through the NOE connectivities shown in Figure 2. Additional NOEs used for complete sequential assignment of HBD-2 included Asp4 β−Pro5 δ, δ′ and Lys40 α−Pro41 δ, δ′ NOEs.

Coupling Constants. Thirteen coupling constants were measured from the DQF-COSY spectrum and were corrected for line broadening. These included one $^3J_{\alpha\beta}$ and 12 $^3J_{HN\alpha}$ coupling constants. The $^3J_{HN\alpha}$ coupling constants are shown in Figure 2.

Slowly Exchanging Amide Protons. For identification of slowly exchanging amide protons in HBD-2, the above NMR sample was lyophilized to dryness and dissolved in 400 μL of H_2O. It was lyophilized again and dissolved in 400 μL of 100% ^2H_2O just prior to data collection. Loss of amide proton signals was observed through an array of one-dimensional spectra and 50 ms TOCSY spectra at 25 °C. The amide protons of those residues for which HN-α cross-peaks were observed after ≥7 h of exchange were identified as slowly exchanging and are denoted in Figure 2.

Conformational Restraints and Structure Calculation. The program Dynamics Algorithm for NMR Applications (DY-

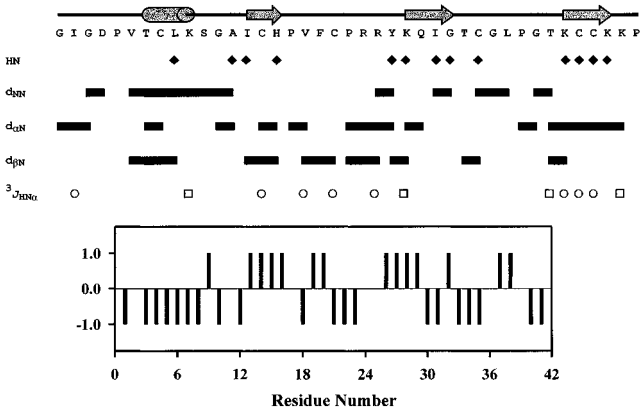

FIGURE 2: HBD-2 secondary structure elements with the cylinder representing the α-helix and the arrows representing the *β*-strands. The sequential HN−HN, Hα−HN, and H*β*−HN NOE connectivities in HBD-2 are depicted as black bars. The black diamonds denote the slowly exchanging amide protons in HBD-2. The white circles and the white squares indicate $3J_{HN\alpha} > 8.0$ Hz and $3J_{HN\alpha} < 6.0$ Hz, respectively. The chemical shift index of α-protons of HBD-2 is shown in the lower part. The chemical shift index classifies α-protons based upon whether their chemical shift is greater than (1), within (0), or less than (−1) the random coil value ± 0.1 ppm. According to the rules of chemical shift index, a group of three or more "1's" not interrupted by a "−1" indicates a *β*-strand and a group of four or more "−1's" not interrupted by a "1" indicates a helix.

ANA) (*24*) was used to generate the necessary distance and dihedral angle constraints based upon the NOE peak volumes with a mixing time of 150 ms and the coupling constants measured from the DQF-COSY spectrum. DYANA was also used to anneal and calculate the structures consistent with these constraints. DYANA uses simulated annealing combined with molecular dynamics in torsion angle space (torsion angle dynamics). Thirteen dihedral angle constraints and 177 distance constraints were used in the structure calculation. Constraints were also added for Cys8−Cys37, Cys15−Cys30, and Cys20−Cys38 disulfide bonds. In addition, all the slowly exchanging amide protons were assigned hydrogen bond donors. Some of the hydrogen bond acceptors were obvious by the distinct NOE connections between the involved residues. The others, including Val6 O−Leu9 HN and Cys8 O−Ala13 HN, were determined by carefully analyzing the interatomic distances between the corresponding donors and potential acceptors in structures calculated without those hydrogen bond constraints. For the slowly exchanging Leu9 HN and Ala13 HN, an alternative method for assigning hydrogen bond acceptors was also used. In this second model, hydrogen bond constraints were added between the partners conventionally expected in a helical configuration, i.e., Leu9 HN−Pro5 O and Ala13 HN−Leu9 O. In DYANA, a total of 100 trial structures were generated for each N-terminal hydrogen bonding model with torsion angles chosen at random. NOE constraints were added to the standard force constant set using the DYANA target function multiplier ω_0 of 10 kJ mol^{-1} Å^{-2}. Torsion angle constraints were added using the default target function multiplier. Each structure was then annealed in 4000 steps from an initial temperature of 8000 K to 0 K, followed by 1000 further steps of conjugate gradient minimization. For each N-terminal hydrogen bonding model, 20 structures with the lowest final target function value were subjected to conformational analysis and averaging using the program Molecule Analysis and Molecule Display (MOLMOL) (*25*).

Table 1: Classification of NMR Distance and Torsion Angle Constraints Used in HBD-2 Structure Calculation

constraint type	no. of constraints
NOE distance constraints	
total	177
intraresidue	75
interresidue	102
1 residue away	69
≥2 and ≤5 residues away	15
>5 and ≤10 residues away	7
>10 residues away	11
<2.50 Å	50
>2.50 and <3.50 Å	73
>3.50 Å	54
torsion angle constraints	
ϕ	12
χ_1	1

RESULTS

To assess the physical state of HBD-2 in solution, static light scattering analysis was performed on seven solutions (five at pH 3.7 and two at pH 6.4) of the peptide ranging in concentration from 2.3 to 10.3 mg/mL. The molecular mass of HBD-2 was determined to be 4500 ± 300 Da with the data sets at pH 3.7 and 6.4 fitting the same line in the Debye plot (Figure 1). Within the limits of experimental error estimated at 6.7%, the observed and calculated (4328.2 Da) molecular masses were the same. Furthermore, dynamic light scattering experiments performed in the same concentration range (data not shown) indicated that there was no dependence of the hydrodynamic size on HBD-2 concentration. The peak value of the hydrodynamic radius distribution was 1.2 nm for all the solutions that were studied. The size distributions that were obtained were narrow and unimodal, indicating the absence of intermolecular aggregates. Thus, at concentrations between 0.5 and 2.4 mM, HBD-2 exists as a monomer in solution.

NMR data collection was carried out at pH 3.7 and 6.4 at a peptide concentration of 0.9 mM. Qualitatively similar spectra were obtained at both pHs. Characteristic NOE contacts between Thr7 and Lys10 were observed at both pHs, indicating the presence of an N-terminal α-helical segment. The structure described below is based on data collected at pH 3.7, because of the better resolution of several α-proton chemical shifts from that of water. Secondary structural features of HBD-2 that emerged from the studies at pH 3.7 are summarized in Figure 2 together with the sequential NOE connectivities, slowly exchanging amide protons and an α-proton chemical shift index (*26*) that documents the structural assignments.

Table 1 shows the classification of the NOE distance constraints and the torsion angle restraints used in HBD-2 solution structure calculations. Violation statistics and the mean global rmsd values for the 20 HBD-2 conformers of each N-terminal hydrogen bonding model are given in Tables 2 and 3, respectively.

According to the first N-terminal hydrogen bonding model (Leu9 HN−Val6 O and Ala13 HN−Cys8 O), HBD-2 contains an α-helical region from residues Thr7 to Lys10, while according to the second model (Leu9 HN−Pro5 O and

Table 2: Violation Statistics for the 20 HBD-2 Conformers of Each N-Terminal Hydrogen Bonding Model

first N-terminal hydrogen bonding model	
mean rms deviations from experimental restraints	
NOE (Å)	0.155 ± 0.005
dihedrals (deg)	3.5 ± 0.4
mean rms deviations from idealized covalent geometry	
bonds (Å)	0.012
angles (deg)	1.7
second N-terminal hydrogen bonding model	
mean rms deviations from experimental restraints	
NOE (Å)	0.161 ± 0.005
dihedrals (deg)	3.5 ± 0.9
mean rms deviations from idealized covalent geometry	
bonds (Å)	0.012
angles (deg)	1.7

Table 3: Mean Global rmsd Values for the 20 HBD-2 Conformers of Each N-Terminal Hydrogen Bonding Model and for the 20 BNBD-12 Structures Available from the Protein Data Bank

residues	backbone rmsd (Å)	heavy atom rmsd (Å)
HBD-2, First N-Terminal Hydrogen Bonding Model		
1−41	1.62 ± 0.41	2.29 ± 0.40
1−13	1.61 ± 0.53	1.95 ± 0.57
13−41	0.91 ± 0.22	1.94 ± 0.36
HBD-2, Second N-Terminal Hydrogen Bonding Model		
1−41	1.39 ± 0.32	2.10 ± 0.32
1−13	1.44 ± 0.51	1.91 ± 0.58
13−41	0.87 ± 0.24	1.86 ± 0.34
BNBD-12		
1−38	2.81 ± 0.90	3.28 ± 0.74
1−10	2.76 ± 0.82	3.78 ± 0.76
10−38	0.93 ± 0.39	1.73 ± 0.49

Ala13 HN−Leu9 O), the α-helical region contains residues Val6−Leu9. The NMR evidence for the presence of this N-terminal α-helix included the characteristic *i* to *i* + 3 NOEs between Thr7 α-Lys10 HN and Thr7 α-Lys10 *β*. Also, *i* to *i* + 1 HN−HN connectivities were observed from Val6 through Ala13, and a negative chemical shift index was observed between residues 3 and 8 and for residue 10.

From Table 3, it can be seen that the rmsds are generally lower for the structures of the second N-terminal hydrogen bonding model than for the structures of the first model.

Two nonsequential NOEs between Asp4 and Cys8 and one between Pro5 and Cys8 also shaped the structure of the N-terminus of HBD-2. Asp4 was assumed to be in the protonated state at pH 3.7, and no change was detected when the structures were calculated with Asp4 in the deprotonated state. Although the amide proton of Thr7 was within hydrogen bonding distance of the Asp4 hydroxy oxygen, it was not found to be slowly exchanging. The Cys8−Cys37 disulfide bond was confirmed by the NOE interactions between the *β*-protons of the two cysteines.

The first strand (*β*1) of the triple-stranded, antiparallel *β*-sheet extends from Ile14 to His16, whereas the third *β*-strand (*β*3) extends from Lys36 to Lys39. The characteristic interstrand backbone NOEs between *β*1 and *β*3 were Ile14 HN−Cys38 HN and His16 HN−Lys36 HN NOEs. Moreover, these four amide protons exhibited slow exchange in ^2H_2O and were constrained in hydrogen bonds between the strands.

Two turns, one consisting of residues Pro17−Cys20 and the other of residues Pro21−Tyr24, follow *β*1 in the solution structure of HBD-2. Both turns are classified as type IV.

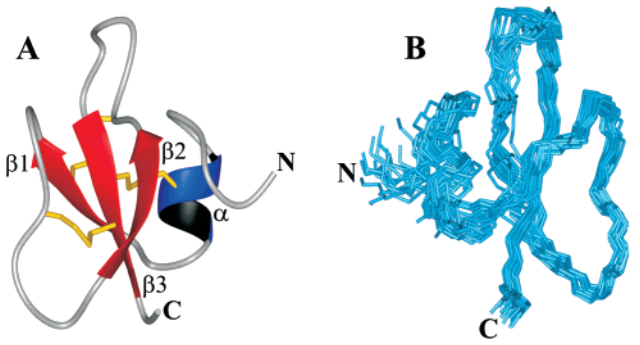

FIGURE 3: Ribbon representation of the HBD-2 conformer of the first N-terminal hydrogen bonding model with the lowest final target function value [MOLMOL (A)] and superposition of the backbones of all 20 HBD-2 conformers of the first N-terminal hydrogen bonding model [MOLMOL (B)].

The global position of the first turn was mainly decided by the NOE connection between Val18 HN and Thr35 α. The sequential Arg23 HN−Tyr24 HN NOE represented the second turn. The amide proton of Tyr24 was found to be slowly exchanging and was constrained in a hydrogen bond with Arg22 O. The side chain NOEs between Tyr24 and Ile14 and those between Tyr24 and Cys38 indicate that the structure is highly ordered at this end of the *β*-region.

The second *β*-strand (*β*2) of the triple-stranded *β*-sheet contains residues Lys25−Gly28 with Ile27 and Gly28 participating in a *β*-bulge. The NMR evidence was strong for the presence of this *β*-bulge. An interstrand backbone NOE was observed between Lys25 HN in *β*2 and Lys39 HN in *β*3. Both these amide protons were slowly exchanging and were constrained in hydrogen bonds between the strands. An *i* to *i* + 1 NOE was observed between Ile27 HN and Gly28 HN. These two amide protons along with Cys37 HN were found to be slowly exchanging. Both Ile27 HN and Gly28 HN were constrained in hydrogen bonds with Cys37 O, while Cys37 HN was constrained in a hydrogen bond with Gly28 O to form a classic *β*-bulge.

Residues Thr29−Thr35 form the loop of the *β*-hairpin involving *β*2 and *β*3. The Thr35 *β* proton exhibited distinct NOEs with Cys30 *β* protons. The sequential Cys30 HN−Gly31 HN, Gly31 HN−Leu32 HN, and Gly34 HN−Thr35 HN NOE connectivities were also observed in this region. Slowly exchanging Cys30 HN was constrained in a hydrogen bond with the hydroxy oxygen of Thr35. Chemical shift index analysis (*26*) of the α protons is summarized in Figure 2 and supports the overall secondary structure assignments for HBD-2.

HBD-2 solution structures depicted in Figures 3−5 are of the first N-terminal hydrogen bonding model. The ribbon form of the HBD-2 conformer with the lowest final target function value and the superposition of the backbones of all 20 conformers are presented in Figure 3. According to the solution structure of HBD-2, the positively charged side chains of Lys10, His16, Arg22, Arg23, Lys25, Lys39, and Lys40 are favorably oriented for solvent accessibility. The hydrophobicity of HBD-2 has been mapped in Figure 4. The figure displays the hydrophilic and hydrophobic faces of HBD-2 distinctly. These observations illustrate the amphiphilic character of HBD-2 and the nonuniform distribution of positive charge at its surface.

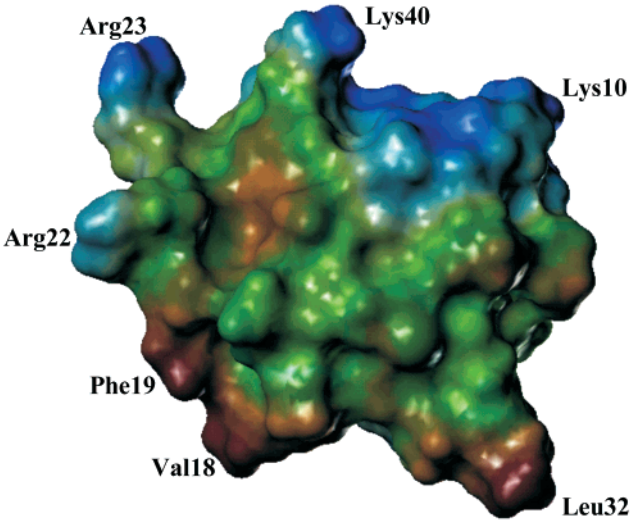

FIGURE 4: Hydrophobicity map of the HBD-2 conformer of the first N-terminal hydrogen bonding model with the lowest final target function value with the hydrophilic areas shown in blue and the hydrophobic areas shown in reddish brown (SYBYL 6.5, Tripos, Inc., St. Louis, MO).

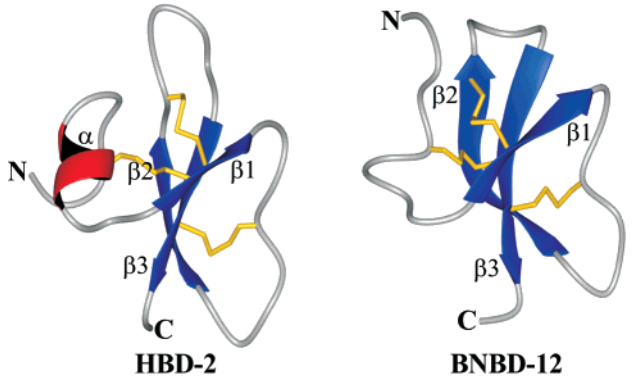

FIGURE 5: Ribbon representations of three-dimensional solution structures (MOLMOL) and sequence alignment of HBD-2 and BNBD-12. The HBD-2 structure shown is of the first N-terminal hydrogen bonding model with the lowest final target function value. The BNBD-12 structure shown is the first of 20 available from the Protein Data Bank.

DISCUSSION

Defensins, because of their cationic nature, are attracted by electrostatic forces to polyanionic structures present in bacterial membranes. This is viewed as the initiating event on a pathway that ultimately leads to disruption of the barrier membrane (*27*). The mechanism by which these bound amphipathic peptides promote the loss of membrane integrity and ultimately cell death remains an area of intense study. An equally intriguing subject is the basis for differences in activity among the various defensins and other peptide antimicrobials toward Gram-negative and Gram-positive bacteria, fungi, yeast, and certain enveloped viruses. Minor structural variation must influence activity in a profound way. In addition to their antimicrobial effects, some defensins attract lymphocytes to sites of inflammation by virtue of a chemokine-like activity. The solution studies of HBD-2 reported here are an important step toward an understanding of the relationships between structure and biological activity of this effector molecule of innate and adaptive immunity.

The NMR structures and the primary sequences of two β-defensins, HBD-2 (pH 3.7, 0.9 mM) and BNBD-12 (pH 4.0, 2.2 mM), are presented in Figure 5. The solution structures are monomeric and similar except for a prominent difference in secondary structure at their amino termini. In the 38-residue BNBD-12 peptide, the N-terminus is reported to consist of a disordered strand followed by an ideal type I β-turn formed by residues Gly6−Gly9 (*16*), although Gly6 α−Gly9 HN and Gly6 α−Gly10 HN NOE connectivities consistent with a helix were observed. The α-proton chemical shift index for residues 1−4, 6, 7, and 9 of BNBD-12 was determined to be −1, 0, 1, −1, 0, −1, and 0, which indicates a random coil structure. In the 41-residue HBD-2 peptide, the corresponding N-terminal region is more ordered with the presence of the α-helical segment. It can be seen from Table 3 that the rmsds in the N-terminal region are much smaller in HBD-2 than in BNBD-12. Several minor structural differences were also apparent on comparison of the bovine and human peptides. The β-sheet content in BNBD-12 is higher than that in HBD-2. This is attributable to the longer β2 and β3 strands in the former structure of six and five residues, respectively. The corresponding β-strand regions of HBD-2 have four residues each. Thus, the β2−β3 interstrand loop region of BNBD-12 is significantly shorter than that in HBD-2. In BNBD-12, the third turn consisting of residues Pro18−Met21 has been specified as a type VI turn with a *cis*-proline at position $i + 2$ and with a hydrogen bond between Met21 HN and Pro18 O. In HBD-2, however, Arg22 O was consistently found to be closer to Tyr24 HN for a hydrogen bond than Pro21 O, and this turn was classified as a type IV turn. Another apparent difference in these structures was identified during the course of exchange studies. In HBD-2, Cys15 was found to be fast exchanging in contrast to the corresponding residue in BNBD-12, Cys12. However, no apparent differences were noted in the β-bulge region where formative residues Ile27, Gly28, and Cys37 in the HBD-2 solution structure corresponded to Ile24, Gly25, and Cys34 in the BNBD-12 structure.

The difference between the N-terminal structures of HBD-2 and BNBD-12 is probably due to the shorter N-terminal segment of BNBD-12 and the presence of a glycine residue at position 6 in the latter structure, for which the corresponding residue at position 9 in HBD-2 is a bulky leucine. The observed differences in N-terminal structure may be a contributing factor to their differences in antimicrobial specificity. For example, BNBD-12 displays greater activity toward *Staphylococcus aureus* (*28*) than HBD-2 (*5*). Indeed, the recent observation by Ouellette et al. (*29*) that the N-termini of murine Paneth cell α-defensins (cryptdins) contribute importantly toward their bactericidal activities supports this notion. It is also possible that the more subtle structural variances noted above may be factors contributing to selectivity differences between these two β-defensins.

Two X-ray structures of HBD-2 were recently reported by Hoover et al. (*18*). In both the monoclinic and orthorhombic crystalline forms, an octameric structure comprised of four HBD-2 dimers is a conserved feature. Our solution structure of HBD-2 is in agreement with the monomeric unit of the crystal structure, including the presence of the novel N-terminal α-helical segment. In our static light scattering

studies conducted at pH 3.7 or 6.4 at concentrations between 0.5 and 2.4 mM, neither HBD-2 dimers nor octamers evident in the crystalline forms of the peptide were observed. The absence of intermolecular NOEs in the NOESY spectra of HBD-2 also indicated the monomeric behavior for HBD-2 in solution at a concentration of 0.9 mM. In contrast, Hoover et al. (*18*) observed principally HBD-2 dimers by dynamic light scattering studies conducted at a HBD-2 concentration of 6.9 mM at pH 8.0. Thus, it is likely that dimerization of HBD-2 in solution requires a threshold concentration of 3.5 mM, i.e., the approximate concentration at which crystals were grown. Previous NMR studies involving the human α-defensin HNP-1 have shown that it exists as a dimer or a higher-order aggregate in solution (*14*, *15*); however, these studies were performed at a HNP-1 concentration approximately 6.5 times higher than the concentration of HBD-2 in our solution structure studies. Thus, insights provided from studies of HBD-2 in solution suggest that at micromolar levels in skin and mucosal secretions, HBD-2 is likely to be present in monomeric form. Moreover, this does not exclude the possibility that multimeric structures of HBD-2 may form at a lipid−water interface at vastly reduced protein concentrations.

In the crystal structure of HBD-2, the N-terminal α-helical region participates in the octameric assembly. The key observation of this work is that the α-helix is also well-defined for the monomer in solution and may, therefore, confer upon the peptide properties important to either its microbicidal or chemokine-like activities or both. According to the X-ray structure of HBD-2, interactions between β1s of two monomers facilitate dimer formation. These interactions include only two hydrogen bonds involving the backbone atoms of Cys15. In our solution structure studies of HBD-2, Cys15 was not observed to be slowly exchanging and no intermolecular NOEs were seen that could implicate the residues of β1 in dimer formation. These findings offer further evidence that HBD-2 is monomeric in solution at the stated limits of concentration.

A β-bulge involving a conserved glycine (Gly28 in HBD-2) is evident in all defensin structures determined to date. In fact, this glycine residue is an invariant feature of every defensin sequence known at present. In the crystal structure of HNP-3, Tyr17 and Gly18 are at the dimer interface (*17*). This suggested that the β-bulge region of other defensins may be similarly involved in promoting dimerization. However, this is conceptually difficult to reconcile with the fact that residues Ile27 and Gly28 that shape the β-bulge evident in the solution structure of HBD-2 have no obvious intermolecular involvement in either the dimeric or octameric crystalline forms of this peptide.

The hydrophobicity map of HBD-2 (Figure 4) suggests a possible mode of action on membranes whereby the highly hydrophobic end would embed itself in the bilayer, leaving the charged and hydrophilic end of the molecule free to interact with the aqueous environment. This would be consistent with a surfactant-like mechanism of action. Future biophysical studies of defensins in the context of model membranes employing oriented CD analysis and solid-state NMR spectroscopy are expected to provide considerable insights into the mechanism by which defensins compromise bacterial barrier membranes.

In summary, the solution structure of HBD-2 showed no evidence of multimer formation in the concentration range of 0.5−2.4 mM and differed from all other known solution defensin structures by the presence of an N-terminal α-helical segment. Future studies of the effects of substitutions in the N-terminal region should clarify its potential contribution to effector functions of HBD-2.

ACKNOWLEDGMENT

We are grateful to Linda L. McCarter, Sue M. Travis, and Michael J. Welsh for their comments on the manuscript. We thank Elena Rus, Brian Morrison, and Dennis Charkowski of the Molecular Analysis Facility and Boyd Knosp of the Image Analysis Facility for their valuable assistance.

REFERENCES

1. Ganz, T., and Lehrer, R. I. (1995) *Pharmacol. Ther. 66*, 191−205.
2. Tang, Y. Q., and Selsted, M. E. (1993) *J. Biol. Chem. 268*, 6649−6653.
3. Ganz, T., and Lehrer, R. I. (1998) *Curr. Opin. Immunol. 10*, 41−44.
4. Schröder, J. M. (1999) *Biochem. Pharmacol. 57*, 121−134.
5. Harder, J., Bartels, J., Christophers, E., and Schröder, J. M. (1997) *Nature 387*, 861.
6. Schröder, J. M., and Harder, J. (1999) *Int. J. Biochem. Cell Biol. 31*, 645−651.
7. Singh, P. K., Jia, H. P., Wiles, K., Hesselberth, J., Liu, L., Conway, B. D., Greenberg, E. P., Valore, E. V., Welsh, M. J., Ganz, T., Tack, B. F., and McCray, P. B., Jr. (1998) *Proc. Natl. Acad. Sci. U.S.A. 95*, 14961−14966.
8. Mathews, M., Jia, H. P., Guthmiller, J. M., Losh, G., Graham, S., Johnson, G. K., Tack, B. F., and McCray, P. B., Jr. (1999) *Infect. Immun. 67*, 2740−2745.
9. O'Neil, D. A., Porter, E. M., Elewaut, D., Anderson, G. M., Eckmann, L., Ganz, T., and Kagnoff, M. (1999) *J. Immunol. 163*, 6718−6724.
10. Harder, J., Meyer-Hoffert, U., Teran, L. M., Schwichtenberg, L., Bartels, J., Maune, S., and Schröder, J. M. (2000) *Am. J. Respir. Cell Mol. Biol. 22*, 714−721.
11. Yang, D., Chertov, O., Bykovskakia, S. N., Chen, Q., Buffo, M. J., Shogan, J., Anderson, M., Schröder, J. M., Wang, J. M., Howard, O. M., and Oppenheim, J. J. (1999) *Science 286*, 525−528.
12. Bach, A. C., II, Selsted, M. E., and Pardi, A. (1987) *Biochemistry 26*, 4389−4397.
13. Pardi, A., Hare, D. R., Selsted, M. E., Morrison, R. D., Bassolino, D. A., and Bach, A. C., II (1988) *J. Mol. Biol. 201*, 625−636.
14. Zhang, X. L., Selsted, M. E., and Pardi, A. (1992) *Biochemistry 31*, 11348−11356.
15. Pardi, A., Zhang, X. L., Selsted, M. E., Skalicky, J. J., and Yip, P. F. (1992) *Biochemistry 31*, 11357−11364.
16. Zimmermann, G. R., Legault, P., Selsted, M. E., and Pardi, A. (1995) *Biochemistry 34*, 13663−13671.
17. Hill, C. P., Yee, J., Selsted, M. E., and Eisenberg, D. (1991) *Science 251*, 1481−1485.
18. Hoover, D. M., Kanaghalagatta, R. R., Blumenthal, R., Puri, A., Oppenheim, J. J., Chertov, O., and Lubkowski, J. (2000) *J. Biol. Chem. 275*, 32911−32918.
19. Valore, E. V., Park, C. H., Quayle, A. J., Wiles, K. R., McCray, P. B., Jr., and Ganz, T. (1998) *J. Clin. Invest. 101*, 1633−1642.
20. Kratochvil, P. (1987) *Classical Light Scattering From Polymer Solutions*, Elsevier Science, Amsterdam.
21. Chu, B. (1991) in *Laser Light Scattering: Basic Principles and Practice*, 2nd ed., p 74, Academic Press, San Diego.
22. Provencher, S. W. (1979) *Makromol. Chem. 180*, 201−209.
23. Wüthrich, K. (1986) *NMR of Proteins and Nucleic Acids*, John Wiley & Sons, New York.

24. Güntert, P., Mumenthaler, C., and Wüthrich, K. (1997) *J. Mol. Biol. 273*, 283−298.
25. Koradi, R., Billeter, M., and Wüthrich, K. (1996) *J. Mol. Graphics 14*, 51−55.
26. Wishart, D. S., Sykes, B. D., and Richards, F. M. (1992) *Biochemistry 31*, 1647−1651.
27. Fujii, G., Selsted, M. E., and Eisenberg, D. (1993) *Protein Sci. 2*, 1301−1312.
28. Selsted, M. E., Tang, Y. Q., Morris, W. L., McGuire, P. A., Novotny, M. J., Smith, W., Henschen, A. H., and Cullor, J. S. (1993) *J. Biol. Chem. 268*, 6641−6648.
29. Ouellette, A. J., Satchell, D. P., Hsieh, M. M., Hagen, S. J., and Selsted, M. E. (2000) *J. Biol. Chem. 275*, 33969−33973.

BI002519D